Hindawi Publishing Corporation
ISRN Aerospace Engineering
Volume 2014, Article ID 409408, 10 pages
http://dx.doi.org/10.1155/2014/409408

Research Article

Designing Stipulated Gains of Aircraft Stability and Control Augmentation Systems for Semiglobal Trajectories Tracking

Mohamed Mostafa Y. B. Elshabasy,[1] Yongki Yoon,[2] and Ashraf Omran[3]

[1] *Department of Mechanical Engineering, Faculty of Engineering, Alexandria University, Alexandria 21544, Egypt*
[2] *Whirlpool Corporation, Saint Joseph Technology Center, 303 Upton Drive, Saint Joseph, MI 49085, USA*
[3] *CNH Industrial, 6900 Veterans Ave., Burr Ridge, IL 60527, USA*

Correspondence should be addressed to Mohamed Mostafa Y. B. Elshabasy; mohamed_elshabasy@alexu.edu.eg

Received 29 August 2013; Accepted 11 December 2013; Published 30 January 2014

Academic Editors: J. Yao and C. Yuan

The main objective of the current investigation is to provide a simple procedure to select the controller gains for an aircraft with a largely wide complex flight envelope with different source of nonlinearities. The stability and control gains are optimally devised using genetic algorithm. Thus, the gains are tuned based on the information of a single designed mission. This mission is assigned to cover a wide range of the aircraft's flight envelope. For more validation, the resultant controller gains were tested for many off-designed missions and different operating conditions such as mass and aerodynamic variations. The results show the capability of the proposed procedure to design a semiglobal robust stability and control augmentation system for a highly maneuverable aircraft such as F-16. Unlike the gain scheduling and other control design methodologies, the proposed technique provides a semiglobal single set of gains for both aircraft stability and control augmentation systems. This reduces the implementation efforts. The proposed methodology is superior to the classical control method which rigorously requires the linearization of the nonlinear aircraft model of the investigated highly maneuverable aircraft and eliminating the sources of nonlinearities mentioned above.

1. Introduction

Due to stringent performance and robustness requirements, modern control techniques have been widely used to design the flight control systems (FCS[s]). However, researchers have been facing the difficulties of the complex nature and the nonlinearity strength embedded in the aircraft's dynamical model. For example, inertia coupling and attitude representations (Euler angles representation or quaternion representation) of the aircraft rigid body motions require nonlinear mathematical models [1]. Special impact on aircraft model comes from the nonlinear aerodynamic submodel such that aerodynamics coefficients significantly change with operating conditions. This leads to a significant change in the stability and performance of the aircraft dynamics. In addition, many other sources of nonlinearities appear in actuator nonlinear subsystems, sensor nonlinear subsystem, and engine nonlinear subsystems.

In order to address the designing FCS, gain scheduling, one of the popular methodologies to design controllers for nonlinear systems has been adopted to design stability augmentation system (SAS), and control augmentation system (CAS) [2–4]. In the conventional gain scheduling approach, the nonlinear system is linearized at several equilibrium operation conditions. Local linear controllers are designed at each of these points. The linear controller gains are then scheduled between the selected equilibrium points to obtain a semiglobal nonlinear controller. There is, however, still a difficulty as to how to schedule the gain from point to point in the operation regime. Even though the gain scheduling method breaks down the nonlinear model into linear models, operating point might have a significant nonlinearity, which cannot be overlooked in the control design. Besides, the selection of the operating points and the design of interpolation scheme remain a time-consuming procedure. There are several approaches to resolve the issue of highly nonlinear

operating conditions such as the dynamic inversion [5], adaptive control [6], and sliding mode control [7]. The more nonlinearity these approaches account for, the more complicated it is to implement the resultant controller on-board. The main goal of this paper is to provide a simple procedure to select the controller gains for an aircraft with a largely wide complex flight envelope such as F-16 with different sources of nonlinearities. Thus, the gains are optimally tuned using genetic algorithm (GA) based on the information for a single designed mission [8–11]. This mission is assigned to cover a wide range of the aircraft's flight envelope. The resultant controller is a semiglobal robust controller and not restricted to any approximation regarding the system's nonlinearity.

Since GA has advantages such as global optimization performance and the ease of distributing its calculations among several processors or computers as it operates on the population of solutions that can be evaluated concurrently, GA is used as an efficient search technique to tune the value of the SAS and CAS controller gains. Thus, there is no need to linearize the model around prescribed patches to design the gains that are only valid for a certain range inside the flight envelope. In other words, the proposed control methodology replaces the classical techniques that depend on scheduling the gains to track the trajectory. Hence, it will be computationally efficient and more realistic because it is based on the nonlinear dynamics of the studied aircraft. To further validate the proposed technique, another mission is tracked using the optimal gains designed by GA to study how close the response of the aircraft is to the off-design mission.

The rest of paper is organized as follows. Section 2 presents the nonlinear dynamic model of F-16 fighter aircraft. Section 3 provides the representation of SAS and CAS. Section 4 reviews the designed flight mission information. Section 5 shows a genetic algorithm to tune the SAS and CAS gains. Section 6 gives the simulation results obtained from the associated nonlinear aircraft model to illustrate the designed-mission/off-designed mission.

2. F-16 Nonlinear Dynamic Model

The F-16 model is considered under many assumptions: the aircraft is a rigid body with six degrees of freedom except for an internal constant spinning engine rotor, the aircraft mass is constant, the aircraft body is symmetric about the XZ plane, the atmosphere is stationary, and the earth is flat with constant gravity. Based on those assumptions, the nonlinear dynamic equations of the F-16 model are first-order ordinary differential equations and can be classified into the following [12, 13] (note that the following variables are listed in the Nomenclature at the end of the paper).

Force equations:

$$\begin{aligned}
\dot{u} &= Rv - Qw - g\sin\theta + \frac{1}{m}\left(\overline{X} + F_T\right),\\
\dot{v} &= Pw - Ru + g\sin\varphi\cos\theta + \frac{1}{m}\left(\overline{Y}\right),\\
\dot{w} &= Qu - Pv + g\cos\varphi\cos\theta + \frac{1}{m}\left(\overline{Z}\right).
\end{aligned} \tag{1}$$

Motion equations:

$$\dot{P} = \left(c_1 R + c_2 P\right)Q + c_3\overline{L} + c_4\left(\overline{N} + H_e Q\right), \tag{2}$$

$$\dot{Q} = c_5 PR - c_6\left(P^2 - R^2\right) + c_7\left(\overline{M} + F_T z_T - H_e R\right), \tag{3}$$

$$\dot{R} = \left(c_8 P - c_2 R\right)Q + c_4\overline{L} + c_9\left(\overline{N} + H_e Q\right). \tag{4}$$

Kinematic equations:

$$\begin{aligned}
\dot{\varphi} &= P + \tan\theta\left(Q\sin\varphi + R\cos\varphi\right),\\
\dot{\theta} &= Q\cos\varphi - R\sin\varphi,\\
\dot{\psi} &= \frac{Q\sin\varphi + R\cos\varphi}{\cos\theta}.
\end{aligned} \tag{5}$$

Navigational equations:

$$\begin{aligned}
\dot{P}_N &= u\cos\psi\cos\theta + v\left(\cos\psi\sin\theta\sin\varphi - \sin\psi\cos\varphi\right)\\
&\quad + w\left(\cos\psi\sin\theta\cos\varphi + \sin\psi\sin\varphi\right),\\
\dot{P}_E &= u\sin\psi\cos\theta + v\left(\sin\psi\sin\theta\sin\varphi + \cos\psi\cos\varphi\right)\\
&\quad - w\left(\sin\psi\sin\theta\cos\varphi + \cos\psi\sin\varphi\right),\\
\dot{h}_E &= u\sin\theta - v\cos\theta\sin\varphi - w\cos\theta\cos\varphi.
\end{aligned} \tag{6}$$

In (2) to (4), the constants $c_i's$,where $i = 1, 2, 3, \ldots, 9$, are defined in terms of the moments of inertias; I_X, I_Y, and I_Z and the product of inertia I_{XZ} are defined as

$$\begin{aligned}
&\Gamma c_1 = \left(I_Y - I_Z\right)I_Z - I_{XZ}^2 \qquad \Gamma c_4 = I_{XZ} \qquad c_7 = \frac{1}{I_Y},\\
&\Gamma c_2 = \left(I_X - I_Y + I_Z\right)I_{XZ} - I_{XZ}^2 \qquad c_5 = \frac{I_Z - I_X}{I_Y},\\
&\Gamma c_8 = I_X\left(I_X - I_Y\right) + I_{XZ}^2\\
&\Gamma c_3 = I_Z \qquad c_6 = \frac{I_{XZ}}{I_Y}I_{XZ} \qquad \Gamma c_9 = I_X,
\end{aligned} \tag{7}$$

where $\Gamma = I_X I_Z - I_{XZ}^2$.

The parameter H_e that exists in the moments equations represents the engine angular momentum which is supposed to be a variable. In the current model, the value of H_e is 160 slug·ft^2/s considering full throttle opening; that is, $\delta_{\text{th}} = 100\%$ [1]. The vehicle mass is denoted by m that is assumed to be constant all the time. g represents the gravitational acceleration $g = 32.2$ ft/s^2. We assume that the thrust produced by the engine, F_T, acts parallel to aircraft's X-body axis, which makes the thrust vector have only one component acting in the X-body axis. In (3), the constant Z_T, which represents the offset distance of the thrust vector away from the cm, is assumed to be zero.

The aerodynamic forces and moments acting on the aircraft $\overline{X}, \overline{Y}, \overline{Z}, \overline{L}, \overline{M}$, and $\overline{N}$ are well described in Roskam [12] and Stevens and Lewis [13]. Force in X-body axis, for example, can be obtained as follows:

$$\overline{X} = \overline{q}SC_{X_T}\left(\alpha, \beta, P, Q, R, \delta_k, \ldots\right), \tag{8}$$

where C_{X_T} is collected from wind tunnel and flight tests.

The total aerodynamic coefficients C_{X_T}, C_{Y_T}, C_{Z_T}, C_{l_T}, C_{m_T}, and C_{n_T} are computed based on the high fidelity aerodynamic data tables in Nguyen et al. (1979). These coefficients are expressed as a baseline component plus a correction terms that are denoted by the symbol δ. The baseline component is primarily a function of angle of attack α, sideslip angle β, and Mach number M. Mach number dependency can be removed from the baseline component and treated as a correction term in the case of data for subsonic speeds. As the available aerodynamic tables (Nguyen et al., 1979) were conducted at subsonic flow conditions, the effect of Mach number was neglected. In this model, the aerodynamic data shows strong dependency on the horizontal stabilizer deflection δ_h; therefore, δ_h was included as an independent variable for the baseline component. Normally, total coefficient equations have been used to sum the various aerodynamic contributions to given force or moment coefficients as listed in (8). The force coefficient C_{X_T}, for example, is defined as (see [1])

$$C_{X_T} = C_X(\alpha, \beta, \delta_h) + \delta C_{X_{\text{lef}}}\left(1 - \frac{\delta_{\text{lef}}}{25}\right) + \delta C_{X_{\text{sb}}}(\alpha)\left(\frac{\delta_{\text{sb}}}{60}\right) + \frac{Q\bar{c}}{2V_T}\left[C_{X_Q}(\alpha) + \delta C_{X_{Q_{\text{lef}}}}(\alpha)\left(1 - \frac{\delta_{\text{lef}}}{25}\right)\right], \tag{9}$$

where

$$\delta C_{X_{\text{lef}}} = C_{X_{\text{lef}}}(\alpha, \beta) - C_X(\alpha, \beta, \delta_h = 0^\circ). \tag{10}$$

In general, the basic rigid dynamics model will contain 12 state variables that are collected in the state vector $\vec{X}$, where

$$\vec{X} = [P_N P_E h : uvw : PQR : \psi\theta\varphi]. \tag{11}$$

The aircraft model has four inputs represented in the control vector $\vec{U}$:

$$\vec{U} = [\delta_{\text{th}} \;\; \delta_h \;\; \delta_e \;\; \delta_r]. \tag{12}$$

Note that the lower limit of the throttle position δ_{th} is set to 5% to prevent the engine surge. Both of δ_{sb} and δ_{lef} are frozen to their neutral positions as they do not have tangible effect on the aircraft dynamics.

3. Autopilot and Augmented Flight Control System

In this research, inner-loop feedback control systems can be grouped into three broad categories which include SAS, CAS, and Fly-by-Wire (FBW) [14]. The SAS was proposed to give suitable damping and natural frequencies to improve the dynamic stability characteristics as they are referred to as dampers, stabilizers, and stability augmenters. However, SAS itself does not provide efficient control output since there might exist undesired output between the pilot's stick input and aircraft response and nonredundancy of the sensors and control circuits which are not able to make the system reliable. Thus, in order to eliminate these phenomena, the CAS added a pilot command input to the flight control computer using a force sensor on the control stick. With CAS, the aircraft dynamic response is typically welldamped, and control response is scheduled with the control system gains to maintain desirable characteristics throughout the flight envelope. With CAS, both dynamic stability and control response characteristics could be tailored and optimized to the mission of the aircraft.

The F-16 aircraft model under investigation has FBW system as a major part of its flight control system. Therefore, the inner-loop feedback control system of the studied model will be referred to as the digital flight control systems (DFCS) throughout the remaining part of this paper [13, 14].

The overall autopilot system shown in Figure 1 needs three commands in each time step, and the system generates horizontal stabilizer, aileron, and throttle command signals that replace pilot commands. At the same time, the rudder control surface is frozen at the neutral position. The autopilot system receives the three commands from the mission generating logic which provides altitude, velocity, and heading angle. In each time step, these three commands are calculated from the flight trajectory that is generated based on the required vehicle motion of each section of the mission [14].

The controller receives 4 input signals, V_c, H_c, R_c, and that ψ_c. Note R_c is zero in this research. The difference between H_c and H signal is passed to a PI controller, $G_H = K_P^H + (K_I^H/s)$. The controller, then, accounts for pitch angle and rate with the two gains K_θ and K_q. The signal is then passed to the actuator dynamic system, which includes position and rate saturation. Also the actuator includes a lag elevator-actuator with time constant $\tau = 0.136$ sec. The feedback loop in the yaw rate channel provides the wash-out filter so that it operates only transiently and does not contribute to a control law when a high frequency is present. Also, in this loop cross-connection called aileron-rudder interconnection (ARI) is implemented via an alpha-dependent gain to achieve a stability axis roll. In heading angle channel, one static gain is chosen to control the heading angle error signal of the actual and desired heading angle. In the feedback loop of velocity channel, error signals of the command and total velocities are tuned with PI controller; $G_{V_T} = K_P^{V_T} + (K_I^{V_T}/s)$.

Addressing the problem, designer needs to find these gains indicated in Figure 1. Linearization of a large system is applicable, but it needs to overlook the different source of nonlinearities such as saturation. Thus, the mission-based controller design is proposed. Upon these considerations, GA will be employed to find such gains in Section 5.

4. Mission Design

To accomplish the searching process for one semiglobal set of SAS and CAS gains, there is a need to design a special mission called a "designed mission." Thus this designed-mission should be assigned to cover a wide flight range of interest. Generating the design mission is considered under the aircraft performance limitations such as maximum rate of climb, maximum roll rate, minimum/maximum speed, actuator limitations, and maximum g-load. Most of these limitations are nonlinearly defined by the operational flight

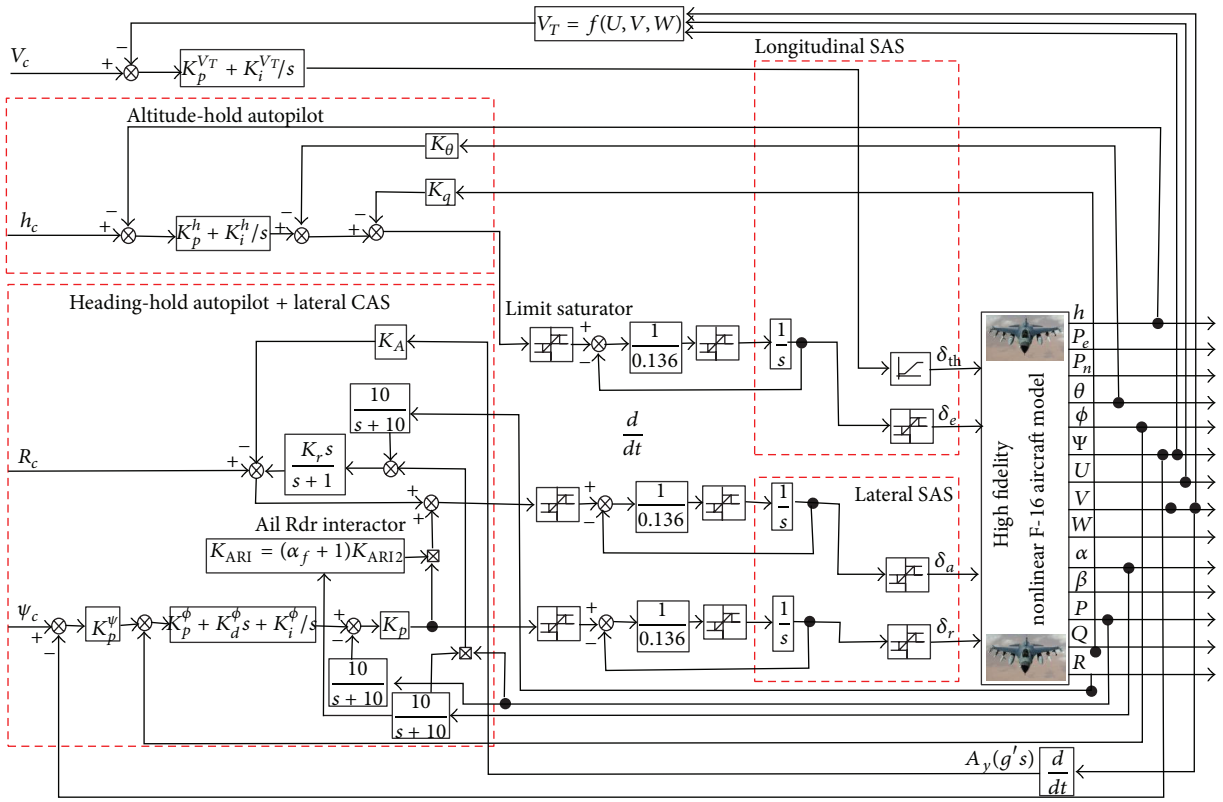

Figure 1: Overall system with autopilot, SAS, and CAS.

conditions (total velocity, altitude, etc.) with coupled hypersurfaces. For example, the definition of maximum rate of climb changes with the altitude is defined as the locus of the weight normalized excess power curve over the energy diagram. Counting these types of such nonlinear constrains leads to increase in the complexity of assigning the designed-mission. For that reason, the mission is initially designed without any extreme attitude that leads to violating the above-listed limits. This mission consists of a set of steering points. The steering points or any combination of the velocity and altitude at any instance of the mission is designed to be completely enclosed inside the flight envelope in order not to violate the structural limit, the stall limit, the propulsive limit, and the atmospheric limits of the flight envelope.

Figure 2, considering these characteristics of aircraft, illustrates the overall flight profile for the aircraft with steering points in terms of time, t_n. The trajectory, S, was assigned by four variables, X, Y, Z, and ψ, in terms of four input variables, $\delta_e, \delta_h, \delta_t$, and δ_a, respectively. Since trajectories of the aircraft can be calculated in terms of time step, profile of total velocity and altitude also can be obtained by the following equations:

$$S(t_i) = \lfloor x(t_i) \quad y(t_i) \quad z(t_i) \quad \psi(t_i) \rfloor,$$
$$V(t_i) = \sqrt{\dot{x}^2(t_i) + \dot{y}^2(t_i) + \dot{z}^2(t_i)}, \tag{13}$$
$$H(t_i) = -z(t_i).$$

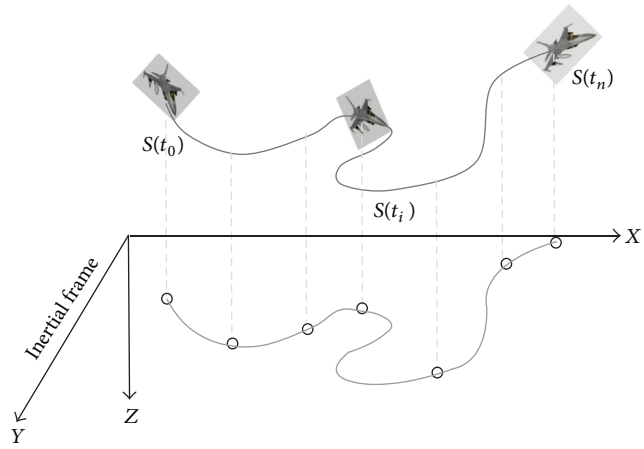

Figure 2: Overview of flight trajectory with/without mission design in the inertial frame.

5. Genetic Algorithm

The genetic algorithm (GA) is used as a global constrained and unconstrained optimization technique which is traced back to 1962 when the algorithm was introduced for studying adaptive systems [9, 10]. The other big advantage of this technique is the ease of distributing its calculations among several processors which is the cornerstone of parallel computation. Moreover, the algorithm is more suited to discontinuous

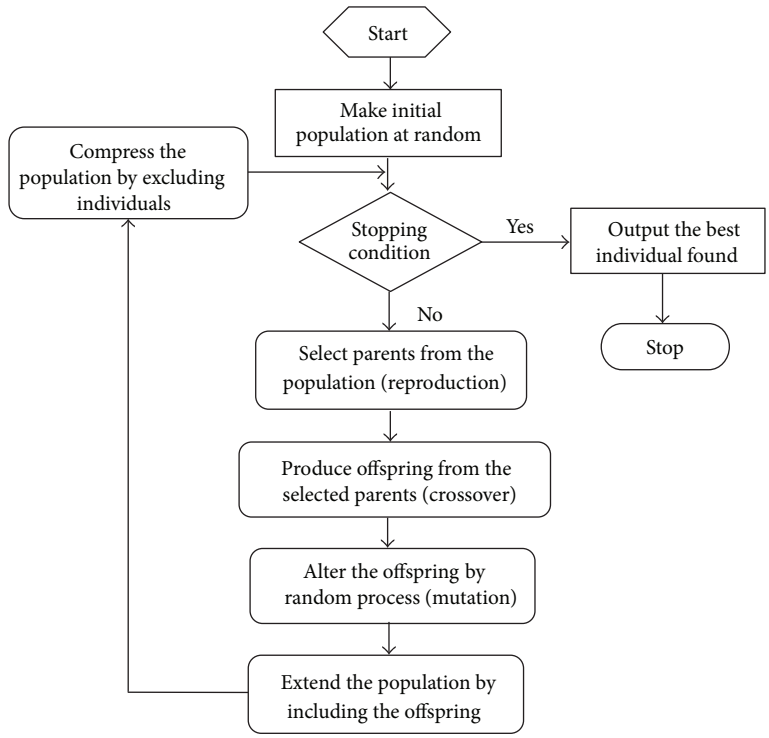

Figure 3: Pseudocode of genetic algorithm.

problems unlike the conventional gradient-based searching algorithms.

Fundamentally, the algorithm logic is based on the process that drives biological evolution (natural selection), where the procedure starts by coding the variables to chromosomes. Every chromosome has n genes. The procedure of the GA is controlled by reproduction, crossover, and mutation processes. Through the reproduction process, the parent is selected from a generation, where the selection process is based on survival of the highest performance index individual. The crossover process is then used to swap between two chromosomes using specific probabilistic decisions. The latter process generates offspring carrying mixed information from swapped parents. To prevent the algorithm from centering on local optimal points, the mutation process is implemented by alternation of the gene from zero to one or from one to zero with the mutation point determined uniformly at random. The mutation rate should be selected carefully such that the algorithm convergence will not last long due to high rate and the algorithm will not converge to a local minimum due to selection of low mutation rate. Roughly, a genetic algorithm works as shown in Figure 3.

The objective function to be optimized is a function in terms of the differences between the desired and the actual values of altitudes, total velocities, and heading angles, respectively, at each designated time step. The objective function is represented as

$$J(\chi) = \frac{1}{\sum_{j=1}^{N} \sum_{i=1}^{4} \left\| y_{ij}^{d} - y_{ij}^{a} \right\|}, \tag{14}$$

where N represents the number of points along the whole mission. Note that y can be arbitrary set that fully describes the mission. In this paper, this set is chosen to be $y = [h \ V_T \ \psi \ R]$ where the commanded yaw rate R was frozen to zero during the whole mission. Such set was chosen to avoid further prekinematic calculations which are out of the scope of the current research. However, for the most of flight motion, the trajectory is defined in terms of the navigation variables that include position and orientation. In (14), the vector $\chi = \left[K_P^{V_T} \ K_I^{V_T} \ K_P^H \ K_I^H \ K_\theta \ K_q \ K_p \ K_P^\phi \ K_P^\psi \ K_r\right]$ denotes the gains of the SAS and CAS. Searching for optimum χ is bounded between χ_{upper} and χ_{lower} where the system is expected to be stable. Assigning these limits is an iterative process as the system is nonlinear.

6. Results

The results of design mission and off-design missions are discussed in detail in this section.

6.1. Results of Design Mission. An air-to-surface mission for a fixed target is designed to simulate a realistic mission of the studied aircraft. This mission represents a simple striking mission that can be training or real mission. The mission consists of climb, cruise, descent, releasing bomb, another sharp climb to escape from the enemy fires followed by very short cruise at relatively high altitude, descent to the original cruise level, and then final descent at the take-off station. The steering points are listed in Table 1. The continuous flight path is generated based on the mission profile, where, at each

Table 1: Velocity, altitude, and heading angle at each steering point.

Steering point	Time (sec)	Altitude (ft)	Velocity (ft/s)	Heading angle (deg)
1	0	1000	540	0
2	100	5000	580	10
3	350	7100	640	80
4	980	7100	700	180
5	1130	1000	810	180
6	1180	1000	820	180
7	1330	20000	790	190
8	1380	20000	760	210
9	1490	17000	750	240
10	1565	17000	750	240
11	1675	14000	690	260
12	1750	14000	620	285
13	2075	1000	540	360

time step, the path consists of sets of three commands—total velocity, altitude, and heading angle. These sets of the three commands are direct input to the autopilot system described before. The autopilot system will follow the prescribed flight path commands through generating the necessary maneuvers for the vehicle. The climb and descent rates and their accelerations are constrained within ±150 ft/s and ±40 ft/s^2, respectively. The heading rate is limited within ±0.027 rad/s, while the angular acceleration of heading angle is limited within ±0.004 rad/s^2. In this research, a nonlinear simulation is developed in order to simulate both systems dynamics and control dynamics using the 4th Runge-Kutta solver. The code of this simulation is executed in the environment of Matlab R2010a through high performance cluster called "Zorka," which has two dual cores of 2.992 GHz Intel Xeon with 8 GB RAM per node. The selected time step is 0.1 second. The time window for simulating the designed-mission is 45 minutes.

The optimal tuning of the controller gains using genetic algorithms starts by generating random initial populations of the controller gains $K_P^{V_T}$, $K_I^{V_T}$, K_P^H, K_I^H, K_θ, K_q, K_p, K_P^ϕ, K_P^ψ, and K_r. The fitness of each individual is evaluated from the inversion of (14). Thus, a genetic algorithm works for maximizing and the control-tuning problem aims to minimize the error. The new generation is selected from the current population and passed to the next iteration of the algorithm. There is a possibility of receiving an unstable behavior for some randomly chosen control gains. In order to avoid such an unstable response, a two-second test simulation is initially conducted to each individual set of gains. If the error during these first 30 seconds violates a specific threshold limit, the simulation will stop and set the fitness value to zero. The parameters of the genetic algorithm are set as follows: (1) the mutation rate is 10%, (2) each generation has a fixed population size of 100 or no generation overlap, and (3) the maximum number of generations is 500. The optimization code was conducted many times with a different starting point (initial solution). In the initial five runs, GA reaches the maximum number of generations without convergence. Starting from the sixth run, GA converges and this convergence is passed to the next run. After the 8th run, even with changing the mutation rate, the gains keep converging at the same values as listed in Table 2.

Table 2: Optimum gain values of the SAS and CAS.

Gains	Values
$K_P^{V_T}$	0.0912
$K_I^{V_T}$	0.0012
K_P^H	0.0661
K_I^H	$1.363e-4$
K_θ	−5.1032
K_q	−9.2311
K_p	0.3230
K_P^ϕ	0.2101
K_P^ψ	−193.62
K_r	−1.9453

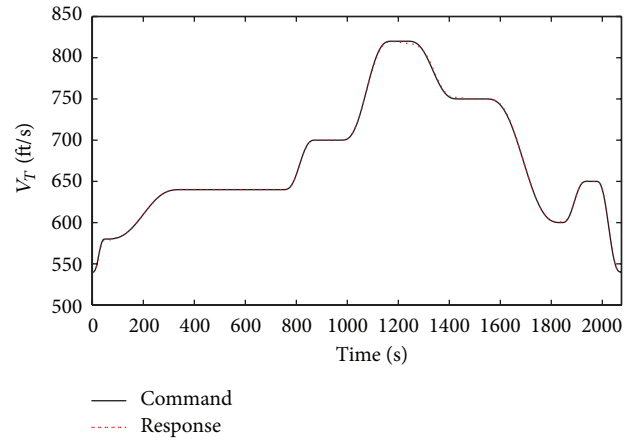

Figure 4: The desired and the response velocities of the F-16 model.

The responses of the aircraft in tracking the designed trajectory are listed in Figures 4, 5, and 6. The variations of elevator, aileron, and rudder are, respectively, plotted in Figure 7. In Figure 7, although the frequencies of variations of the aileron or the rudder look high, the zoom-in views show that the cycle time is about 10 sec. Moreover, the maximum range of the cycle is almost 0.15 deg for the aileron and 0.07 deg for the rudder (see Figure 7). For insight analysis of the variations of the aircraft's states during the mission, the time history of each state is plotted in a separate figure. Based on these results, it can be noticed that variation in the control surfaces is close to the deflection values at the trimming conditions. The variations of the roll and pitch angles ϕ, θ during the whole missions are plotted in Figure 8. The angular rates P, Q, and R are plotted versus the time for the whole

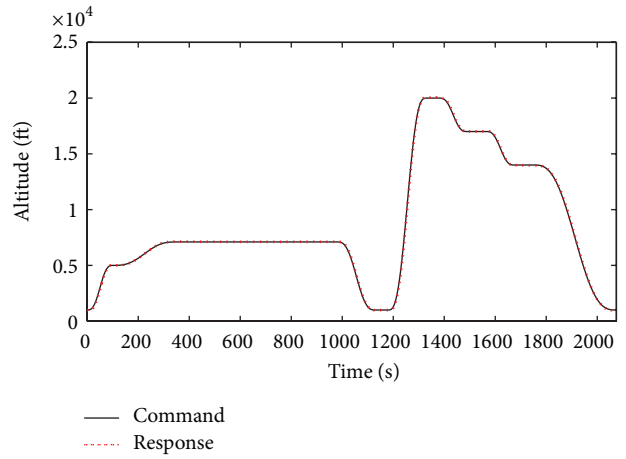

Figure 5: The desired and the response altitudes of the F-16 model.

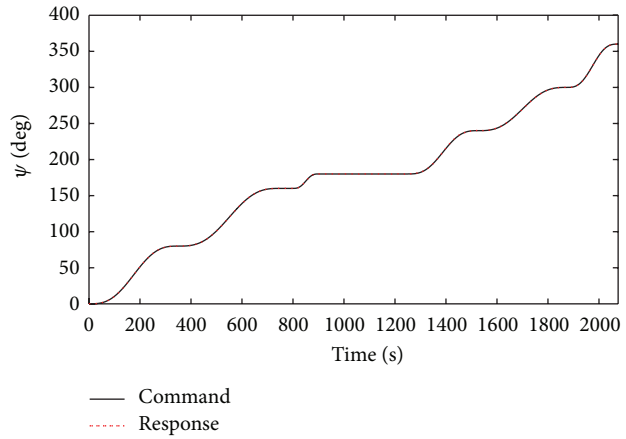

Figure 6: The desired and the response heading angles of the F-16 model.

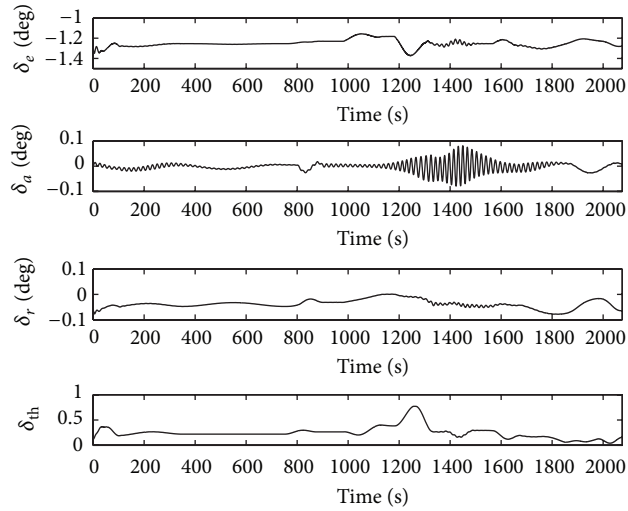

Figure 7: The elevator, aileron, rudder, and throttle's variation with time during the on-design mission, respectively.

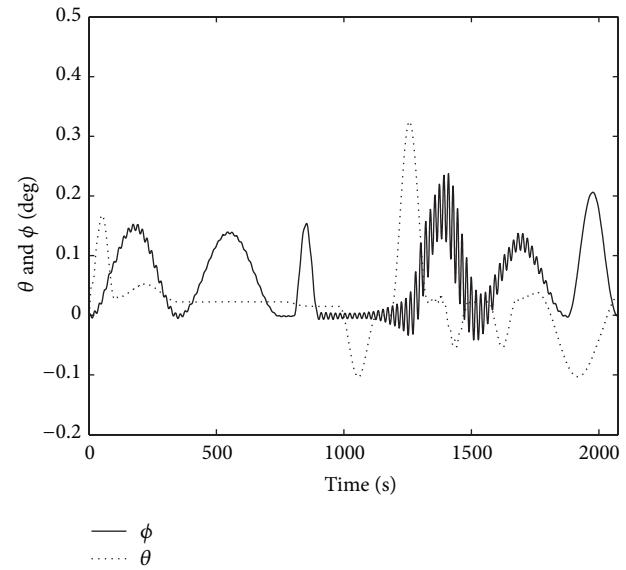

Figure 8: The variation of roll and pitch angles with time during the on-design mission.

mission in Figure 9. Notice that none of the control surfaces approaches its mechanical limits [1].

6.2. Results for Off-Design Missions. Now, the resultant mission-based controller using GA is validated for an off-designed mission. Figure 10 shows the difference between the selected off-designed mission and the designed mission in terms of the trajectories of altitudes, total velocities, and the heading angles of the off-design mission. These two mission start from the same position, "O," and end at different ones based on missions.

In order to provide a more realistic simulation of the off-designed mission, system uncertainties and sensor noises are considered [15]. Table 3 shows the standard deviations of sensor noise for the total velocity, altitude, attack angle, and rates of roll, pitch, and yaw. Note that uncertainty was chosen of only 10% increments for the certain parameters which are mass and moment of inertia about X-body axis I_{xx}, while considering 5% decrements of pitching moment coefficient "C_{mT}" and thrust. In Figures 11 and 12, the normalized deviations between actual and desired values of total velocity, altitude, and heading angle were shown with or without noise and uncertainty. Overall, there exists sharp change in certain time frame for velocity and heading angle of the aircraft, while the altitude keeps smooth change over the time range. Figure 13 represents how actual velocity response including noise and uncertainty behaves comparing to command velocity.

7. Conclusion

Using the genetic algorithm to select constant gains during the prescribed missions within a specific patch inside the flight envelope is more efficient than the traditional gain scheduling control scheme. The steps of gain scheduling

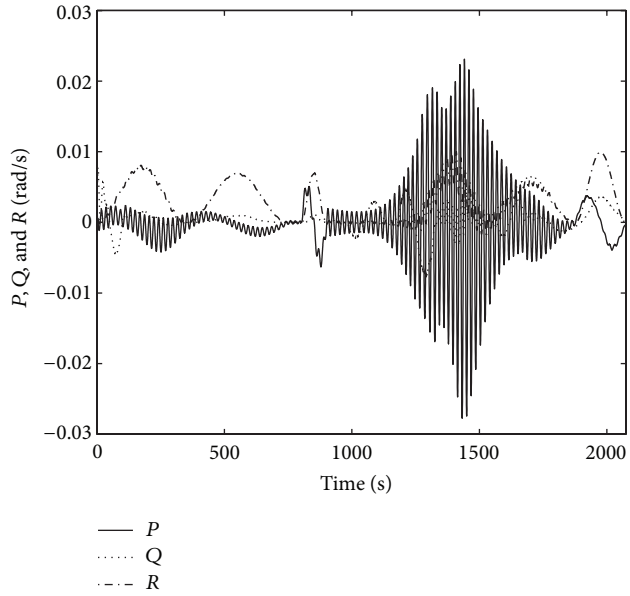

Figure 9: The variation of roll, pitch, and yaw rates with time during the on-design mission.

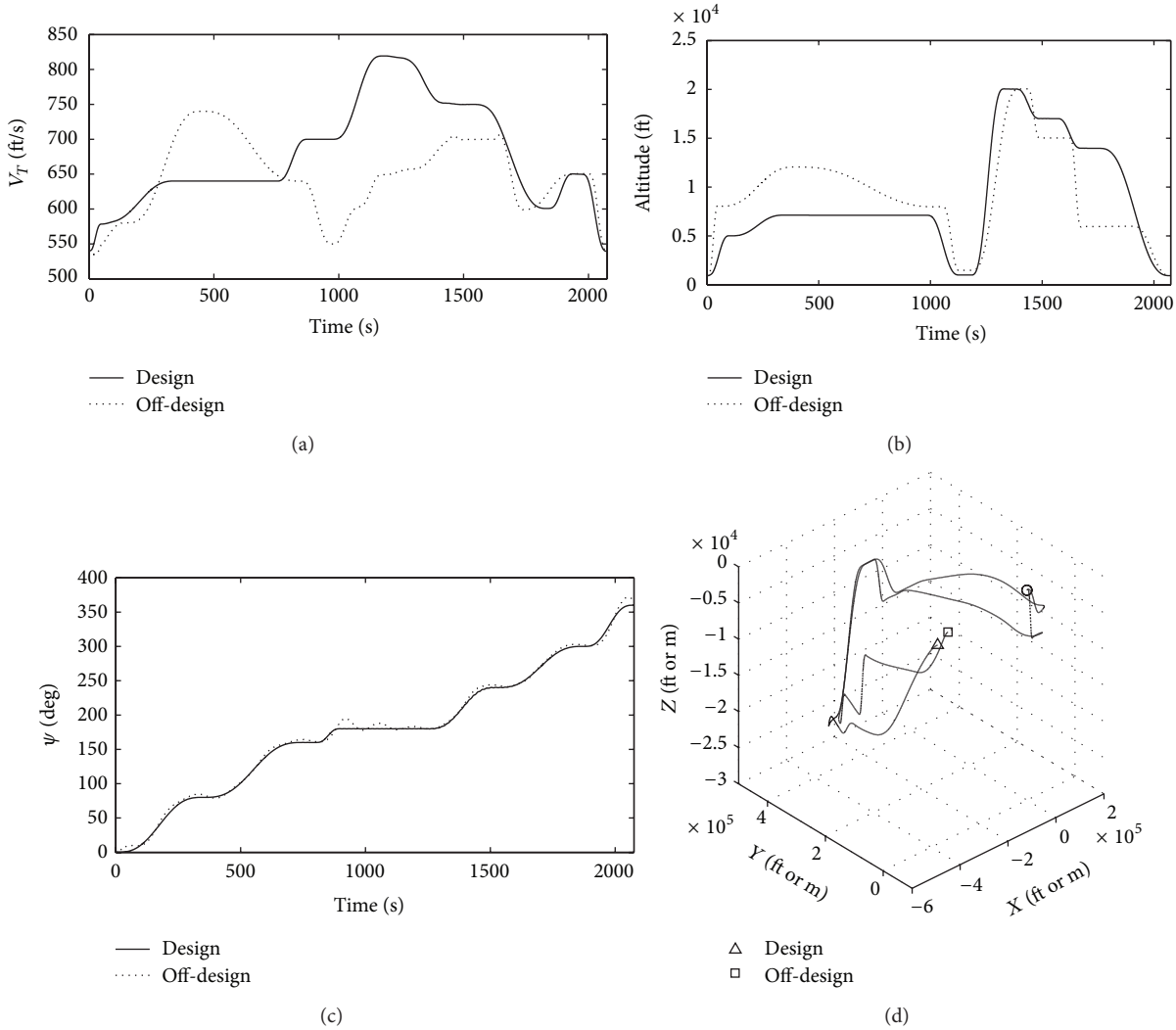

Figure 10: Total velocities, altitudes, heading angles, and flight trajectories of design/off-design mission without noise and uncertainty.

Table 3: Magnitude of sensor noise standard deviations.

Parameter	Standard deviation
Airspeed indicator	11 ft/sec
Roll rate gyro	0.14 deg/sec
Pitch rate gyro	0.14 deg/sec
Yaw rate gyro	0.14 deg/sec
Longitudinal accelerometer	0.98 ft/sec^2
Lateral accelerometer	0.98 ft/sec^2
Directional accelerometer	0.98 ft/sec^2
Attitude pitch gyro	0.573 deg
Attitude roll gyro	0.573 deg
Attitude yaw gyro	0.573 deg
Altitude rate indicator	0.25 ft/sec
Altitude indicator	10 ft
Angle of attack	0.1 deg
Sideslip angle	0.1 deg

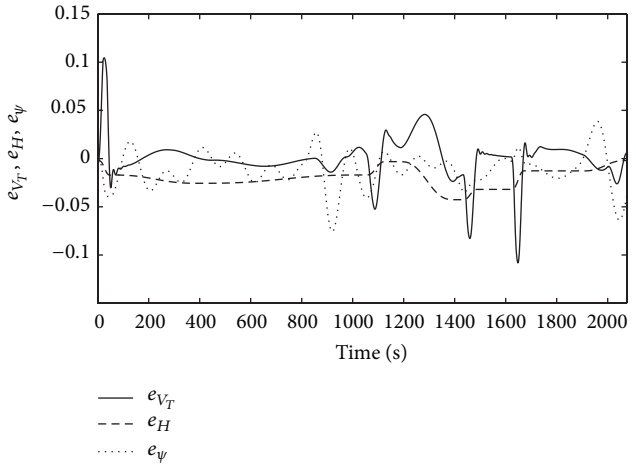

Figure 11: Normalized errors of total velocity, altitude, and heading angle of off-design mission without noise and uncertainty.

process make it numerically costly as the control system is based upon linearization of the aircraft nonlinear motions around various points along the mission. Moreover, more insight analysis of the dynamics model is mandatory for the acceptable results. On the contrary, the genetic-optimized cost function depends on the errors between the desired and the actual trajectories of the prescribed mission without the time-consuming profound analysis of the aircraft dynamics at various points along certain mission. The genetic-select gains can be used with different off-design missions inside the envelope of the design mission.

Nomenclature

u, v, w: Velocity components in x, y, and z body axes (ft/s)
P, Q, R: Airplane roll, pitch, and yaw rates (rad/s or deg/s)
M: Mach number (dimensionless)

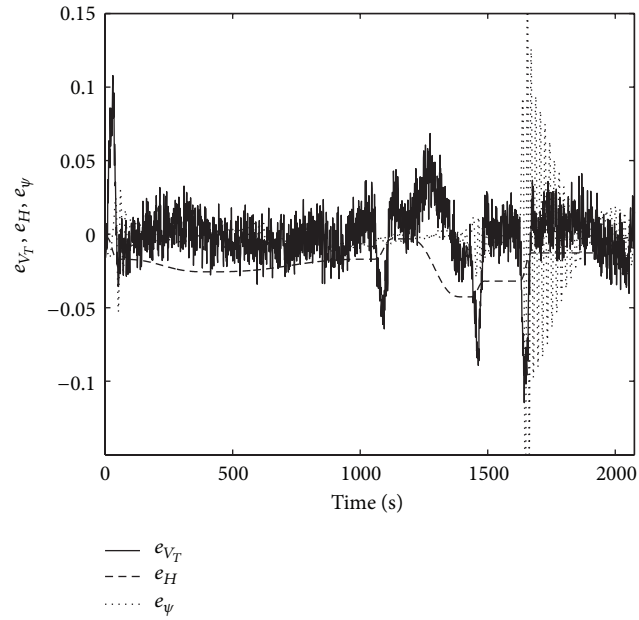

Figure 12: Normalized errors of total velocity, altitude, and heading angle of off-design mission with noise and uncertainty.

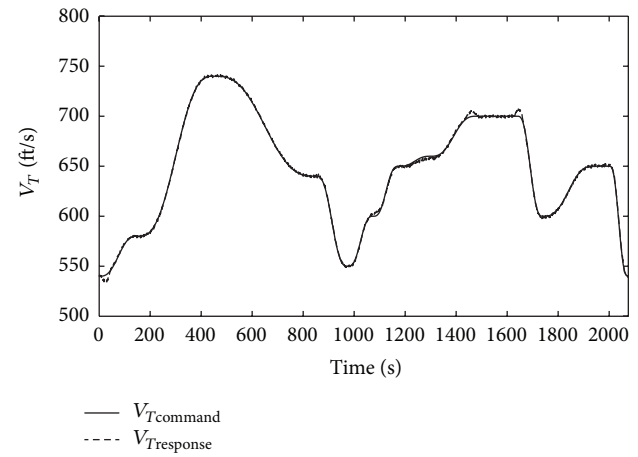

Figure 13: The desired and command velocities with noise and uncertainty.

F_T: Total instantaneous engine thrust, horizon time (Ib)
h_E: Altitude (ft)
P_N, P_E: Aircraft position in north and east (ft)
H_e: Engine angular momentum (slug·ft^2/s)
$\overline{X}, \overline{Y}, \overline{Z}$: Aerodynamic force in XYZ body axis (Ib)
$\overline{L}, \overline{M}, \overline{N}$: Aerodynamic moment in XYZ body axis (Ib.ft)
$\overline{q}$: Free stream aerodynamic pressure (Ib/ft^2)
α: Angle of attack (deg)
β: Sideslip angle (deg)
ψ: Heading angle (deg)

φ, θ: Roll and pitch angles (deg)
I_X, I_Y, I_Z: Moment of inertia about X, Y, and Z body axes (slug·ft^2)
I_{XZ}: Product of inertia with respect to X and Z body axes (slug·ft^2)

V_T: Aircraft total velocity (ft/s)
δ_h: Elevator deflection (deg)
δ_{lef}: Leading edge flap deflection (deg)
δ_{sb}: Speed breaker deflection (deg)
θ_{th}: Throttle percentage (dimensionless)
$C_{X_T}, C_{X_Y}, C_{X_Z}$: Total X, Y, and Z axis force coefficients (dimensionless)
$C_{l_T}, C_{m_T}, C_{n_T}$: Total rolling, pitching, and yawing moment coefficients (dimensionless).

Disclosure

The second and third authors would like to acknowledge that the presented work in this paper does not belong or represent their current affiliations at any level.

Conflict of Interests

The authors declare and certify that there is no conflict of interests regarding the publication of this research paper.

References

[1] L. T. Nguyen, M. E. Ogburn, W. P. Gilbert, K. S. Kibler, P. W. Brown, and P. L. Deal, "Simulator study of stall/ post stall characteristics of a fighter airplane with relaxed longitudinal static stability," NASA TP-1538, NASA, Washington, DC, USA, 1979.

[2] T. Richardson, P. Davison, M. Lowenberg, and M. di Bernardo, "Control of nonlinear aircraft models using dynamic state-feedback gain scheduling," in *Proceedings of the AIAA Guidance, Navigation, and Control Conference and Exhibit*, AIAA-2003-5503, Austin, Tex, USA, August 2003.

[3] M. N. Hammoudi and M. H. Lowenberg, "Dynamic gain scheduled control of an F16 model," in *Proceedings of the AIAA Guidance, Navigation and Control Conference and Exhibit*, AIAA-2008-6487, Honolulu, Hawaii, USA, August 2008.

[4] W. J. Rugh and J. S. Shamma, "Research on gain scheduling," *Automatica*, vol. 36, no. 10, pp. 1401–1425, 2000.

[5] S. A. Snell, D. F. Enns, and W. L. Garrard Jr., "Nonlinear inversion flight control for a supermaneuverable aircraft," *Journal of Guidance, Control, and Dynamics*, vol. 15, no. 4, pp. 976–984, 1992.

[6] G. J. Balas, "Flight control law design: an industry perspective," *European Journal of Control*, vol. 9, no. 2-3, pp. 207–226, 2003.

[7] E. Promtun and S. Seshagiri, "Sliding mode control of pitch-rate of an F-16 aircraft," *International Journal of Engineering and Applied Sciences*, vol. 5, article 1, 2009.

[8] J. Holland, *Adaptation in Natural and Artificial Systems: An Introductory Analysis with Applications to Biology, Control, and Artificial Intelligence*, University of Michigan Press, Ann Arbor, Mich, USA, 1992.

[9] E. Goldberg, *The Design of Innovation: Lessons from and for Competent Genetic Algorithms*, Kluwer Academic, Norwell, Mass, USA, 2002.

[10] C.-D. Yang, C.-C. Luo, S.-J. Liu, and Y.-H. Chang, "Applications of Genetic-Taguchi algorithm in flight control designs," *Journal of Aerospace Engineering*, vol. 18, no. 4, pp. 232–241, 2005.

[11] A. Omran and A. Kassem, "Optimal task space control design of a Stewart manipulator for aircraft stall recovery," *Aerospace Science and Technology*, vol. 15, no. 5, pp. 353–365, 2011.

[12] J. Roskam, *Airplane Flight Dynamics and Automatic Controls*, University of Kansas, Lawrence, Kan, USA, 6th edition, 2001.

[13] B. L. Stevens and F. L. Lewis, *Aircraft Control and Simulation*, Wiley-Interscience, New York, NY, USA, 2nd edition, 2003.

[14] V. R. Schmitt Morris, J. W. Morris, and G. D. Jenny, *Fly-by-Wire: A Historical and Design Perspective*, Society of Automotive Engineers, 1998.

[15] P. Motyka, W. Bonnice, S. Hall, E. Wagner et al., "The evaluation of failure detection and isolation algorithms for restructurable control," NASA Contractor Report 177983, National Aeronautics and Space Administration, Langley Research Center, Hampton, Va, USA, 1985.